THE JOURNAL OF BIOLOGICAL CHEMISTRY VOL. 292, NO. 6, pp. 2379–2394, February 10, 2017

Allosteric Transmission along a Loosely Structured Backbone Allows a Cardiac Troponin C Mutant to Function with Only One Ca^{2+} Ion*

Received for publication, October 28, 2016, and in revised form, December 28, 2016 Published, JBC Papers in Press, January 3, 2017, DOI 10.1074/jbc.M116.765362

Mayra de A. Marques[‡1], Jose Renato Pinto[§2], Adolfo H. Moraes[¶], Anwar Iqbal[‡], Mariana T. Q. de Magalhães[‖], Jamila Monteiro[‡], Murilo M. Pedrote[‡], Martha M. Sorenson[‡3], Jerson L. Silva[‡4], and Guilherme A. P. de Oliveira[‡5]

From the [‡]Programa de Biologia Estrutural, Instituto de Bioquímica Médica, Instituto Nacional de Biologia Estrutural e Bioimagem, Centro Nacional de Ressonância Magnética Nuclear Jiri Jonas, Universidade Federal do Rio de Janeiro, Rio de Janeiro 21941-902, Brazil, the [§]Department of Biomedical Sciences, College of Medicine, Florida State University, Tallahassee, Florida 32304, the [¶]Departamento de Química, Instituto de Ciências Exatas, Universidade Federal de Minas Gerais, Belo Horizonte, Minas Gerais 31270-901, Brazil, and the [‖]Departamento de Bioquímica e Imunologia, Universidade Federal de Minas Gerais, Belo Horizonte, Minas Gerais 31270-901, Brazil

Edited by Roger J. Colbran

Hypertrophic cardiomyopathy (HCM) is one of the most common cardiomyopathies and a major cause of sudden death in young athletes. The Ca^{2+} sensor of the sarcomere, cardiac troponin C (cTnC), plays an important role in regulating muscle contraction. Although several cardiomyopathy-causing mutations have been identified in cTnC, the limited information about their structural defects has been mapped to the HCM phenotype. Here, we used high-resolution electron-spray ionization mass spectrometry (ESI-MS), Carr-Purcell-Meiboom-Gill relaxation dispersion (CPMG-RD), and affinity measurements of cTnC for the thin filament in reconstituted papillary muscles to provide evidence of an allosteric mechanism in mutant cTnC that may play a role to the HCM phenotype. We showed that the D145E mutation leads to altered dynamics on a μs-ms time scale and deactivates both of the divalent cation-binding sites of the cTnC C-domain. CPMG-RD captured a low populated protein-folding conformation triggered by the Glu-145 replacement of Asp. Paradoxically, although D145E C-domain was unable to bind Ca^{2+}, these changes along its backbone allowed it to attach more firmly to thin filaments than the wild-type isoform, providing evidence for an allosteric response of the Ca^{2+}-binding site II in the N-domain. Our findings explain how the effects of an HCM mutation in the C-domain reflect up into the N-domain to cause an increase of Ca^{2+} affinity in site II, thus opening up new insights into the HCM phenotype.

Hypertrophic cardiomyopathy (HCM)[6] is the most common familial heart disorder. Macroscopic features include myocardial disarray and left ventricle thickening accompanied by significant calcium imbalance at a molecular level (1, 2). The relationship between a myosin heavy chain (*MYH7*) gene defect and HCM was a groundbreaking discovery that identified HCM as the first cardiac disease linked to an inherited defect. Subsequent reports identified mutations encoding primarily for sarcomeric proteins (3). New mutations in *TNNC1* (A8V, A31S, and D145E), the gene that codifies cardiac troponin C (cTnC), have been observed in patients with HCM (4, 5).

Cardiac troponin C, a subunit of the troponin complex (Tn), is a key player in regulating muscle contraction at the level of the thin filament (6, 7) and belongs to the EF-hand family of Ca^{2+}-binding proteins. The EF-hand motif is known for its highly conserved helix-loop-helix structure consisting of 12 amino acids organized spatially to coordinate Ca^{2+} or Mg^{2+} in a pentagonal bipyramidal arrangement. cTnC comprises two globular domains with a pair of EF-hand motifs in each domain. The N-domain Ca^{2+} affinity ($\sim 10^5$ M^{-1}) is lower than that of the C-domain ($\sim 10^7$ M^{-1}) (8). Moreover, the N-domain site I has lost a Ca^{2+}-coordinating carboxylate moiety (9), so that myofilament contraction is triggered by the binding of a single Ca^{2+} ion to site II. The binding of Ca^{2+} to this site leads to the exposure of hydrophobic patches and a slight opening that favors interaction with troponin I (7).

HCM-causing mutations can lead to changes in the cTnC three-dimensional structure and tend to impair its ability to regulate the Ca^{2+} binding process and interact with biological partners on the thin filament (10). The single-residue substitution at position 8 in the N-helix of cTnC (A8V) confers an increase of the α-helical content (11). Although the overall ^1H-^{15}N HSQC spectrum appears similar to that of the wild-type

* This work was supported by Grant SAXS-14200 from the Brazilian Synchrotron Light Laboratory and Grant RMN-15571 from the Brazilian Biosciences National Laboratory. This work was also supported by grants from the National Council of Technological and Scientific Development (CNPQ), the Ministry of Health (MS/Decit), and the Carlos Chagas Filho Foundation for Research Support in the State of Rio de Janeiro (to J. L. S.). The authors declare that they have no conflicts of interest with the contents of this article. The content is solely the responsibility of the authors and does not necessarily represent the official views of the National Institutes of Health.

[1] Recipient of a doctoral fellowship from CNPQ.
[2] Recipient of National Institutes of Health Grant HL128683.
[3] Recipient of a CNPQ research fellowship.
[4] Recipient of a CNPQ research fellowship. To whom correspondence may be addressed. E-mail address: jerson@bioqmed.ufrj.br.
[5] Supported by the Cancer Foundation and the Carlos Chagas Filho Foundation for Research Support in the State of Rio de Janeiro. To whom correspondence may be addressed. E-mail address: gaugusto@bioqmed.ufrj.br.

[6] The abbreviations used are: HCM, hypertrophic cardiomyopathy; TnC, troponin C; cTnC, cardiac troponin C; ESI-MS, electron-spray ionization mass spectrometry; CPMG-RD, Carr-Purcell-Meiboom-Gill relaxation dispersion; bis-ANS, 4,4′-dianilino-1,1′-binaphthyl-5,5′-disulfonic acid; CSP, chemical shift perturbation(s); SAXS, small-angle X-ray scattering; NSD, normalized spatial discrepancy; PDB, Protein Data Bank.

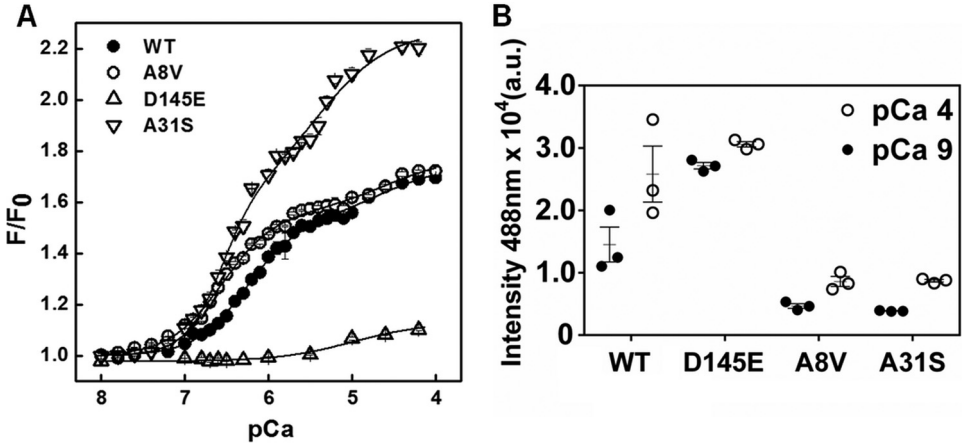

FIGURE 1. **D145E C-domain adopts an open conformation.** *A*, Ca^{2+} titrations in WT and HCM-related mutants. F_0 corresponds to the background fluorescence of cTnC with bis-ANS at 488 nm before the addition of Ca^{2+}. *p*Ca represents $-\log[Ca^{2+}]$. *Black lines* show fittings with a two-transition sigmoidal equation. *B*, bis-ANS fluorescence at λ_{max} (*i.e.* 488 nm) at *p*Ca 9.0 and 4.0 for WT and studied mutants. Each point shows independent experiments. *Bars* represent the average ± S.E.

(WT) form, this mutation seems to increase the population of the N-domain open conformation (12). In the case of A31S, the subject carrying this mutation is prone to develop ventricular fibrillation. Although little is known about the structure of A31S, the secondary structure content is the same as that observed for WT, and in reconstituted fibers, Ca^{2+} affinities and force development are increased (5). The cTnC D145E mutation carries an extra methylene at the Z+ position of the coordinate sphere at site IV. This mutation increases Ca^{2+} affinity of the N-domain site and force recovery in reconstituted fibers (4) but drastically decreases Ca^{2+} binding to the C-domain. To our knowledge, no studies have addressed, at the structural level, the mechanism of how decreased Ca^{2+} affinity in the D145E C-domain would lead to the paradox of increased affinity of the Ca^{2+}-binding site II in the N-domain and its associated effects on the HCM phenotype. The structural consequences of HCM-causing mutations not specifically associated with alterations in the Ca^{2+} coordination sphere (*i.e.* A8V in the N-helix and A31S in the loop of the defunct Ca^{2+}-binding site I) were explored for comparison.

Among the main physiological changes associated with cardiomyopathies, the altered concentration of intracellular Ca^{2+} is a common feature, reflecting the fact that cTnC is one of the major Ca^{2+} buffers in the cardiomyocyte. A lower affinity of the C-domain for Ca^{2+} in the cTnC variant (D145E) compared with the WT protein has been reported (13). Here, using an ensemble of thermodynamic and structural approaches including steady-state fluorescence, circular spectropolarimetry, NMR spectroscopy, and electron-spray ionization mass spectrometry (ESI-MS) we describe how altered Ca^{2+} binding to the C-domain of D145E impacts cTnC function in solution and in permeabilized fibers. Based on ESI-MS and nuclear spin relaxation data, the results suggest that D145E impairs both of the Ca^{2+}-binding sites of the cTnC C-domain: site IV, due to a direct effect of the mutation at the coordination sphere, and site III as a side effect of the altered dynamics triggered by eliminating Ca^{2+} at site IV. Carr-Purcell-Meiboom-Gill relaxation dispersion (CPMG-RD) measurements have captured a low populated protein-folding intermediate that is not present in the WT isoform and promotes tighter cTnC binding to permeabilized fibers. Based on our results and previous functional studies with D145E (4, 13), we provide evidence for an allosteric mechanism occurring between the two lobes of cTnC. Our findings explain how the effects of an HCM mutation in the C-domain reflect up into the N-domain to cause an increase of Ca^{2+} affinity in site II, thus opening up new insights into the HCM phenotype.

Results

D145E Lacks Ca^{2+}-induced Hydrophobic Changes—To examine the overall profile of Ca^{2+} binding, we performed Ca^{2+} titrations on WT cTnC and three HCM-related mutants (A8V, A31S, and D145E) using bis-ANS (4,4′-dianilino-1,1′-binaphthyl-5,5′-disulfonic acid) fluorescence. As shown in Fig. 1*A*, all curves except that for D145E were biphasic. Following an abrupt increase from *p*Ca ~7.0 to 5.5 or 5.0, there was a second transition from *p*Ca ~5.0 to 4.0. The magnitudes of these transitions were the same for WT and A8V (F/F_0 = 1.69 and 1.73, respectively), showing that conformational changes associated with hydrophobic exposure during Ca^{2+} binding were similar (Fig. 1*A*). In contrast, the magnitude for A31S was much greater (F/F_0 = 2.20), indicating higher hydrophobic exposure upon Ca^{2+} binding to the C-domain (Fig. 1*A*). The first transition for A31S was also greater than for the other proteins. Although the first transition was not observed for D145E, the fluorescence magnitude of the second transition was comparable to that for WT and A8V, showing that the hydrophobic exposure of the N-domain was not affected by the mutation (Fig. 1*A*). Evaluation of bis-ANS emission curves at *p*Ca 9.0, the Ca^{2+}-deficient form (apo), and 4.0, the Ca^{2+}-saturated form (holo), revealed a greater hydrophobic exposure of D145E compared with WT at *p*Ca 9.0, suggesting that the apo-D145E C-domain is already in an open conformation (Fig. 1*B*). A8V and A31S led to only modest exposure of hydrophobic patches at *p*Ca 9.0 and 4.0 when compared with the WT. All curves except that for D145E were fit to two classes of binding sites to obtain K_1 and K_2 (Table 1).

TABLE 1
Affinity constants for Ca^{2+} binding to C-domain (K_1) and N-domain (K_2) of cTnC
K_1 and K_2 are expressed as average ± S.E. ($n = 3$ independent experiments).

cTnC	K_1	K_2
	pCa	*pCa*
WT	6.27 ± 0.02	4.66 ± 0.14
A8V	6.55 ± 0.05[a]	4.62 ± 0.12
A31S	6.58 ± 0.03[a]	5.41 ± 0.07[a]
D145E	ND[b]	4.98 ± 0.05[a]

[a] $p < 0.05$ compared with their respective WT values.
[b] ND, not determined.

D145E Inactivates the Binding of Two Ca^{2+} Ions in Cardiac TnC—In a previous report (13), similar data obtained with bis-ANS binding to WT, A8V, and D145E proteins were interpreted as reporting first, Ca^{2+} binding to C-domain sites (lacking D145E), and second, nonspecific Ca^{2+} binding to weak Ca^{2+}/Mg^{2+} sites (non-EF-hand) of the C-domain. None of the bis-ANS signal was assigned to the N-domain, and the question of whether the D145E mutation inactivates site IV was left open (13). To answer this question, we first analyzed the chemical shift perturbations (CSP) obtained by comparing *p*Ca 2.5 against *p*Ca 7.0 (N-domain sensitivity) and *p*Ca 6.0 against *p*Ca 7.0 (C-domain sensitivity) through ^{1}H-^{15}N peak assignments (Figs. 2 and 3). CSP plots for WT and D145E revealed differences in perturbed residues in both proteins (Fig. 4*A*). At low Ca^{2+} concentration (*p*Ca 6.0–7.0) CSP values that differed by ≥1 S.D. from the average across all evaluated residues were mapped onto the cTnC structure. There were several differences in the C-domain between WT and D145E (Fig. 4*B*), distinguishing the two isoforms and pinpointing structural changes triggered by Ca^{2+} binding. Of note, the N-domain response was also different. For the Ca^{2+} range of high-affinity sites (*p*Ca 6.0–7.0), residues Lys-17, Leu-48, Gln-58, Asp-75, and Met-80 are mapped onto the WT N-domain, whereas Ala-23, Phe-27, and Glu-66 are shown at right for the mutant (Fig. 4*B*). It is evident that structural changes in the N-domain due to Ca^{2+} in the WT C-domain are different from the structural changes produced in the D145E N-domain. For the Ca^{2+} range of low-affinity sites (*p*Ca 2.5–7.0), several N-domain residues affected in WT were also affected in D145E, including Asp-25, Gly-30, Gly-34, Gly-42, and Gly-70, but perturbation of Gly-140 and Asp-149 in the C-domain was only observed for the mutant (Fig. 4*B*). The structural differences mapped here reveal sharp differences in the effect of Ca^{2+} on the structure of the C-domain of D145E.

To confirm our hypothesis that Ca^{2+} binding to cTnC C-domain is drastically affected in D145E, we performed high-resolution mass spectrometry analyses of both the WT and D145E prepared in the absence and presence of Ca^{2+}. First, the accurate molecular mass of WT and D145E in the absence of Ca^{2+} was determined by MALDI-TOF/MS. The WT and D145E forms revealed m/z values of 18,401.5 and 18,415.5 Da, respectively, and a $\Delta m/z$ of 14 Da, as expected for incorporation of the methylene group due to the aspartic to glutamic acid substitution (Figs. 4*C* and 5, *A* and *B*). We next designed ESI-MS runs for WT and D145E under both the absence (2 mM EGTA) and presence of Ca^{2+} (4 mM Ca^{2+}, no Mg^{2+}) to measure the binding of Ca^{2+} by quantifying the average molecular masses. Our results revealed peak average m/z values of 18,756.6 and 18,873.4 Da for WT apo- and holoforms, respectively, and a difference between them of 116.8 Da. D145E apo- and holoforms differed by 41.1 Da, with peak average m/z values of 18,941.6 Da for the apoform and 18,982.7 Da for the holoform (Figs. 4*C* and 5, *C–F*, and Table 2). Our results show that D145E has lost the ability to bind two Ca^{2+} ions.

Increase of Thermal Stability of Cardiac TnC Is Governed by Ca^{2+} Binding to C-domain Sites—To characterize the thermal stability of WT and HCM variants, using circular dichroism we monitored the loss of secondary structure generated by rising temperatures. The apo-states of all three mutants exhibited a similar sigmoidal transition with an increase in temperature that could be fit as a three-state process. In the holo-state, only D145E maintained the three-state behavior observed for its apoform. Reversibility was observed for all constructs, and the melting temperatures at the midpoint for the first and second transitions (T_m) were extracted (Fig. 6). In the holo-state, because of increased stability for WT, A8V, and A31S, the second transition was not observed. Thus only one T_m value was extracted for this condition. Statistical significance for these differences was observed for WT against A31S ($p = 0.041$) and D145E ($p = 0.0003$) (Fig. 6). There was no difference in the thermostability of D145E in the absence or presence of Ca^{2+}. These results show that the binding of Ca^{2+} to the C-domain sites of cTnC governs the increase of thermostability. The mutant, unable to bind Ca^{2+} at these sites, retains the two-transition profile of apo-cTnC.

Lower Stability of D145E Does Not Affect Overall Cardiac TnC Structure—A detailed overview of how the mutation at Asp-145 affects the cTnC global conformation was obtained using dihedral angle restraints based on HN, $H_{\alpha,\ H\beta,\ \text{and}}$ ^{15}N chemical shifts and the software TALOS+ to provide backbone *phi* and *psi* angles (14). The α-Helix and β-sheet contents were similar for D145E and WT, revealing that although the mutation impairs Ca^{2+} coordination, it does not affect protein secondary content (Fig. 7*A*). The interatomic function $P(r)$ describes the distribution of distances r between pairs of points within a given volume (the protein particle). The expected $P(r)$ distribution for a bilobular protein such as cTnC is a major peak at low values of r followed by a prominent shoulder at higher values of r, as clearly observed for all three holovariants. There were no significant differences in dimensional values extracted from $P(r)$ distributions when comparing WT and D145E in the holo-state (Fig. 7, *B–D*). In contrast, higher D_{max} values were obtained for the apo-states, as summarized in Table 3. Tertiary contacts were investigated by small-angle X-ray scattering (SAXS), creating a scattering profile of each protein in its apo- and holo-states (Fig. 8). Our results indicate that the mutations studied in the holo-state (A8V, A31S, and D145E) do not affect the overall conformation of cTnC. The effect of Ca^{2+}-binding impairment on D145E stability is better observed when the protein is challenged by 5 M urea, in the holo- and apo-states. As shown on the Kratky plots, in the presence of 5 M urea, the bell shape of the WT holo-state contrasts with the WT apoform, whereas D145E is similar in both states (Fig. 7*E*). A continuous increase in $I(s)^*s^2$ values as a function of s in the Kratky plots is consistent with an unfolding process. Altogether our data sug-

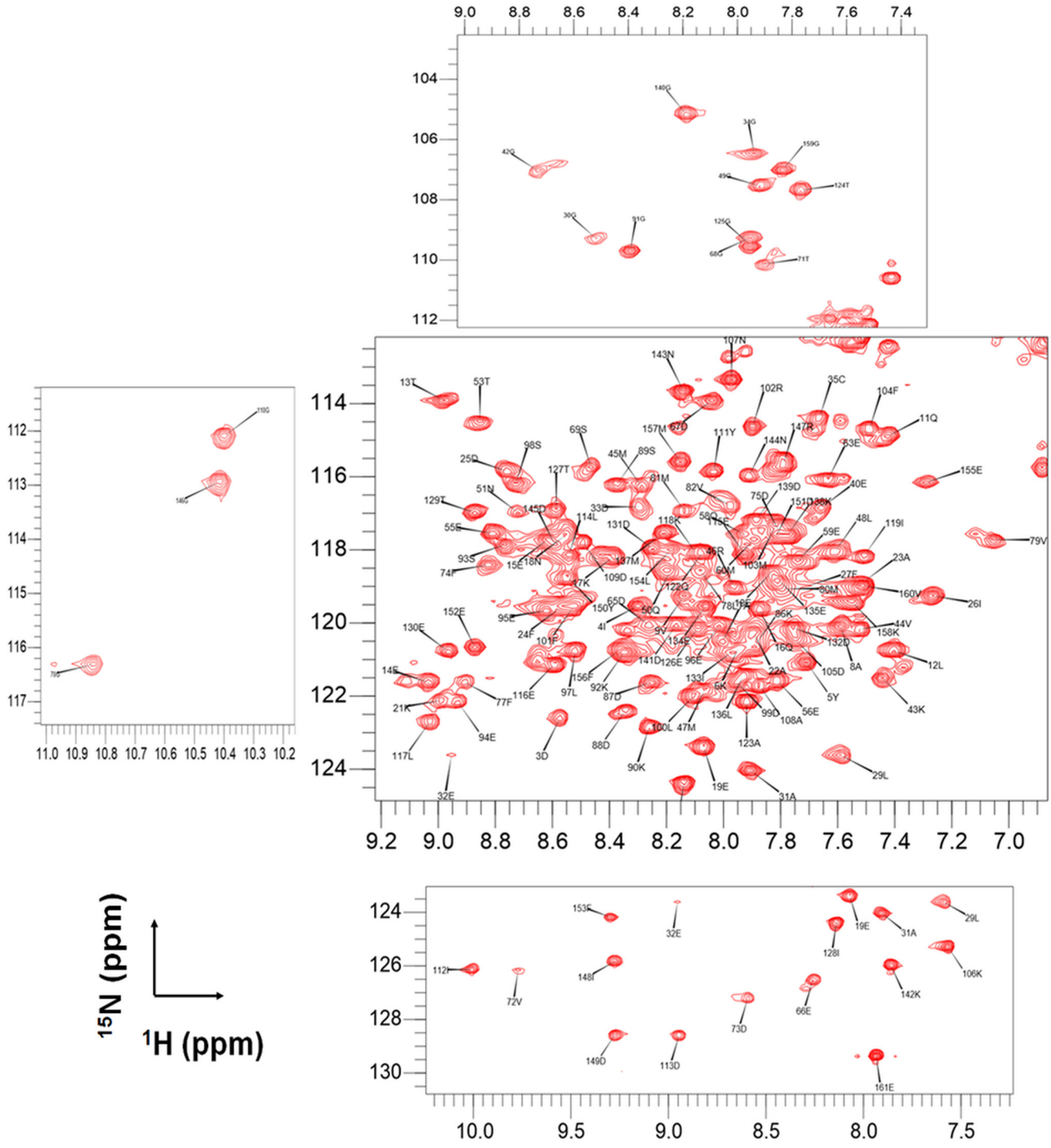

FIGURE 2. **^{1}H-^{15}N HSQC spectrum showing the backbone assignment of NH cross-peaks for holo-WT cTnC.**

gest that the D145E mutation does not affect the global secondary and tertiary contacts but has lower stability because of local changes that arise from impaired Ca^{2+} binding.

D145E Affects C-domain Local Dynamics—Because D145E does not affect the overall secondary and tertiary structure of the protein but does affect Ca^{2+} binding and stability, we designed a protocol for obtaining a complete set of backbone dynamics by measuring amide ^{15}N longitudinal (R_1) and transverse (R_2) relaxation times and ^{1}H-^{15}N heteronuclear NOE (Fig. 9, {^{1}H}-^{15}N NOE). When the data were plotted to show the R_2/R_1 ratio per residue, WT and D145E were markedly different (Fig. 9*A*, *upper panel*). R_2/R_1 values $\geq$ 1 S.D. from the average across all evaluated residues indicate conformational exchange motions on a μs-ms time scale. In D145E, several residues located in α-helix D (αD) (Asp-75, Phe-77, Val-79, Met-81, and Val-82), αE (Arg-102), αF (Leu-114 and Thr-124), αG (Met-137 and Gly-140), and αH (Phe-153, Glu-155, Met-157, and Gly-159) revealed values of R_2/R_1 more than 1 S.D. above the average (4.08 $\pm$ 0.71) (Fig. 9, *B* and *C*). This means that there are distinct regions along the backbone from αD to αH where N-H

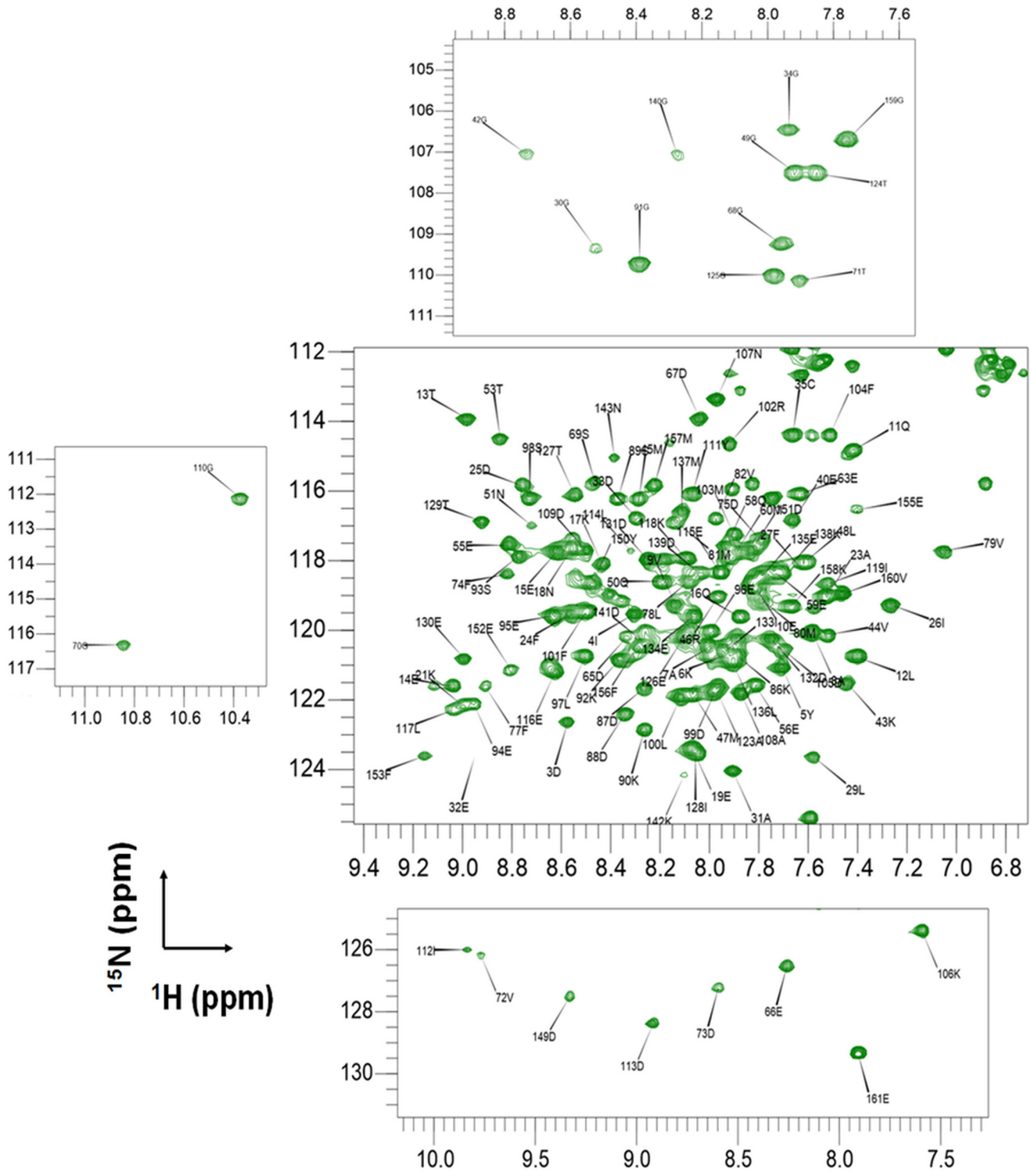

FIGURE 3. **^{1}H-^{15}N HSQC spectrum showing the backbone assignment of NH cross-peaks for holo-D145E cTnC.**

motions are slower for the mutant, presumably because of repercussions from loss of Ca^{2+} binding and lower stability. Of note, helices G and H flank the last EF-hand-binding site (site IV) in the C-domain. Moreover, several αD residues in the N-domain sense these slower dynamics occurring in the C-domain (Fig. 9*B*).

Another type of information resides in the ^{1}H-^{15}N heteronuclear NOE values for each residue, which are related basically to internal motions of ^{1}H-^{15}N bonds on a much faster (ps-ns) time scale. These values were similar for WT and D145E, with average values across all residues of 0.55 ± 0.18 and 0.53 ± 0.22, respectively (Fig. 9*A*, *lower panel*). The N- and C-terminal segments of both proteins presented lower NOE values, a sign of increased flexibility at these sites. In addition, residues 87–91, forming the loop that connects the N- and C-domains, displayed negative values consistent with its flexible behavior (31).

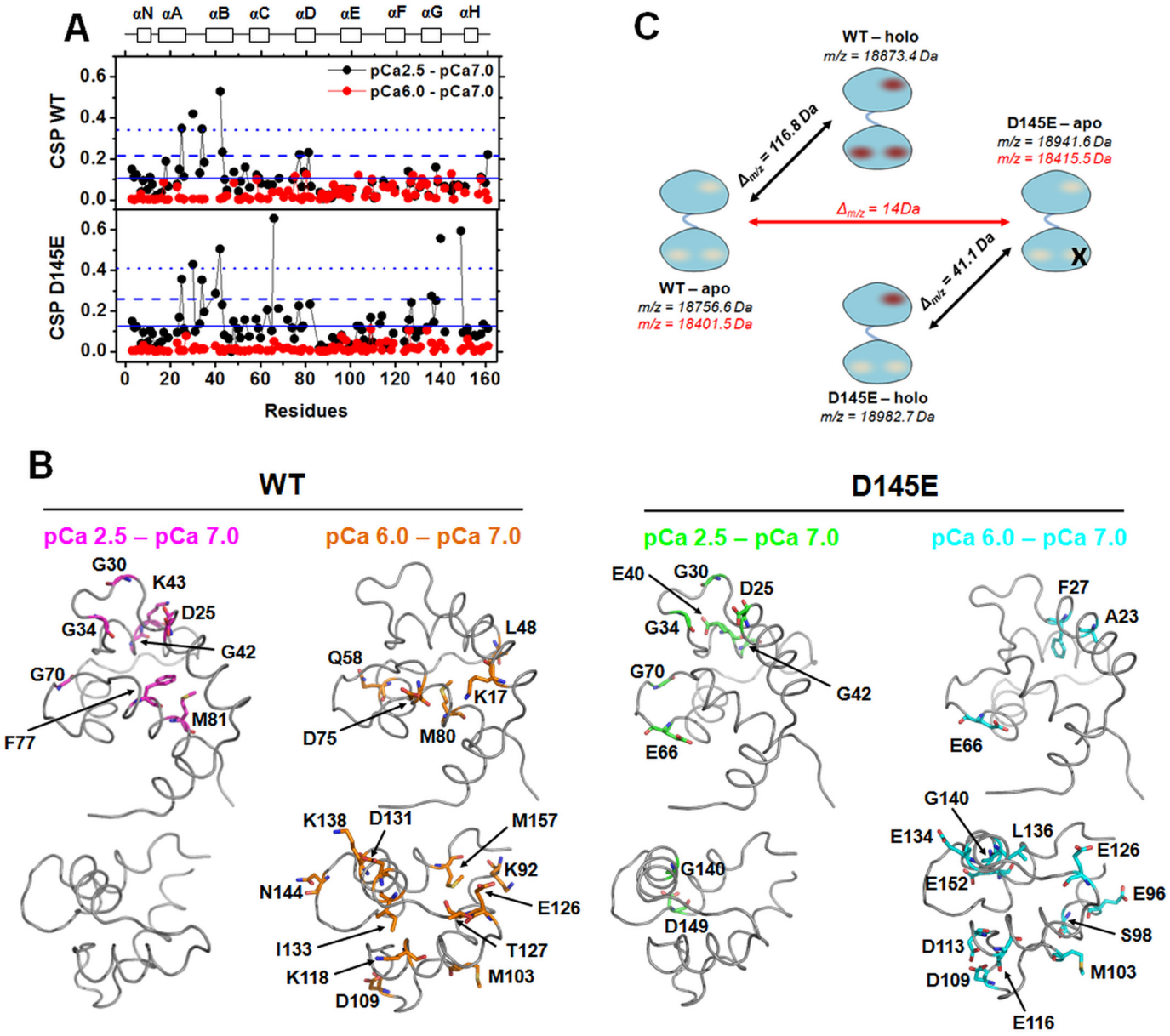

FIGURE 4. **D145E eliminates the binding of two Ca^{2+} ions in cTnC.** *A*, CSP plots as a function of residue, comparing *p*Ca 2.5 (*black*) and pCa 6.0 (*red*) against *p*Ca 7.0 for WT and D145E. Average values of CSP among residues ± S.D. were 0.104 ± 0.114 for *p*Ca 2.5 WT, 0.131 ± 0.138 for *p*Ca 2.5 D145E, 0.033 ± 0.036 for *p*Ca 6.0 WT, and 0.018 ± 0.022 for *p*Ca 6.0 D145E. *Solid*, *dashed*, and *dotted blue lines* show average CSP values for *p*Ca 2.5, average ± 1 S.D., and average ± 2 S.D., respectively. *B*, residues exhibiting CSP values greater than 1 S.D. above the average taken across all evaluated residues are *highlighted* in different *stick colors* in the cTnC subunit (*gray ribbon*) of the cTn complex (PDB code 1J1E) for WT and D145E at both studied *p*Ca values. The structure is tilted at different angles for better visualization of the highlighted residues. *C*, schematic representation of MALDI-TOF/MS (*red*) and ESI-MS (*black*) *m/z* and Δ*m/z* values for WT and D145E in apo- and holo-states. The *X* marks the position of the mutation in Ca^{2+}-binding site IV. Empty Ca^{2+}-binding sites are shown in *gray* and filled sites in *red*.

Interestingly, the NOE values for these residues tended to be more negative for D145E compared with WT, indicating a more flexible linker (Fig. 9*D*). Conformational exchange motions on a μs-ms time scale were not present in the WT, and the R_2/R_1 values were not uniformly distributed among residues (Fig. 9*A*, *upper panel*), which is consistent with the presence of different correlation times (τ_{c1} and τ_{c2}) for tumbling of the N (residues 1–90)- and C-domains (residues 91–161) of WT cardiac TnC (Fig. 9*E*).

To quantify the conformational changes in D145E, we turned to ^{15}N CPMG-RD measurements, which are sensitive to millisecond exchange dynamics. The effective decay constant of magnetization (R_{2eff}) evaluated at 25 and 37 °C with refocusing pulses of 50 and 1000 Hz revealed intermediate exchange motions for D145E at both temperatures on the order of milliseconds that were not observed for WT cTnC. Of note, these movements, visible for residues 125–157 in the *D145E panels* of Fig. 10*A*, were even more pronounced for D145E at 37 °C. Additionally, at 37 °C some residues of WT acquired fast-exchange motions (μs time scale), observed as virtually identical values of R_{2eff} for the two refocusing pulses of 50 and 1000 Hz. These fast-exchange motions indicate that some residues in the WT N-domain (Asp-3, Glu-14, Gly-30, Glu-32, and Gly-42) do develop fast-exchange motions when challenged at physiologi-

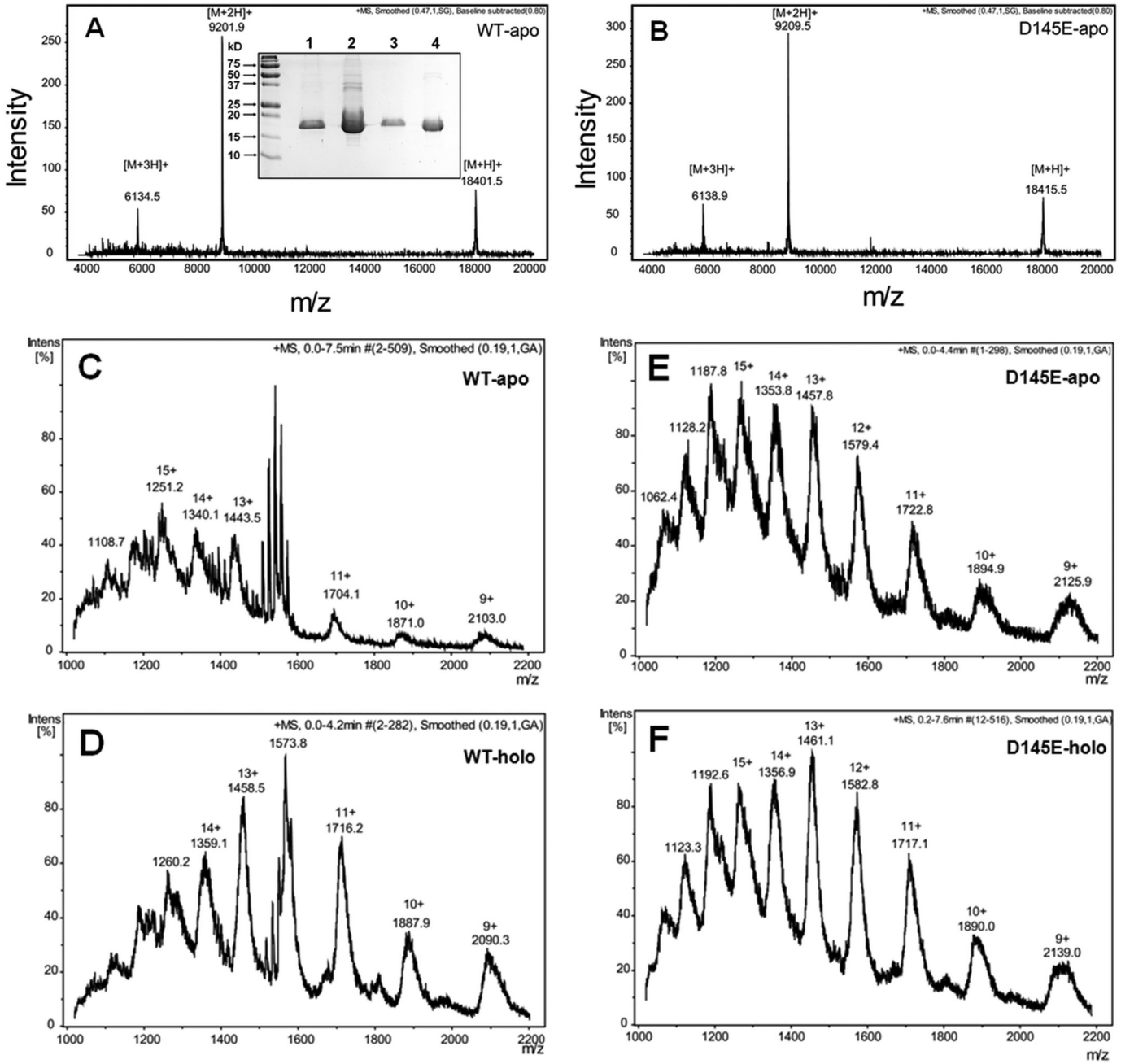

FIGURE 5. **SDS-PAGE and ESI-MS analysis of WT and D145E.** *A* and *B*, the accurate molecular masses and purity of ^{15}N cTnC WT (*A*) and D145E (*B*) were determined by MALDI-TOF/MS. Samples were prepared in the absence of Ca^{2+}. *A*, *inset* shows an SDS-PAGE to demonstrate protein purities. *Lanes*: *1*, WT; *2*, WT 5× concentrated; *3*, D145E; *4*, D145E 5× concentrated. *C–F*, the average molecular masses and binding of Ca^{2+} to WT and D145E were determined by ESI-MS analysis (Table 2). All samples were mixed in similar molar concentrations, and direct injection was performed at a constant flow rate (0.4 ml · min^{-1}) using 50% acetonitrile. Intensity (%) is shown as a function of *m/z* for ^{15}N-cTnC WT apo (*C*) and holo (*D*) and D145E apo (*E*) and holo (*F*).

cal temperatures (Fig. 10*B*). Strikingly, residues experiencing a conformational exchange on the intermediate time scale (ms motions) in D145E were clustered close to the loop of Ca^{2+}-binding site III (Thr-127, Thr-129, and Asp-131) and along the αH helix (Asp-149, Asp-151, Phe-153, Glu-155, Met-157, Lys-158, and Gly-159) at the extreme C terminus of the protein (Fig. 10*B*). From the CPMG-RD experiments at 37 °C, we observed 11 residues of D145E that showed relaxation dispersion profiles with conformational exchange contributions for $R_{2\text{eff}}$ in the intermediate time scale (Arg-102, Thr-127, Thr-129, Asp-131, Asp-132, Lys-138, Asp-149, Tyr-150, Phe-153, Met-157, and Lys-158). Fig. 10*C* shows representative relaxation dispersion profiles for Arg-102, Asp-131, Lys-138, and Met-157 recorded on spectrometers of 500 and 800 MHz and fitted for a two-state model (see "Experimental Procedures"). Our relaxation dispersion measurements have captured for D145E a conformational exchange state between the native state (*N*) and a high energy state occurring with exchange rates of $K_{\text{ex}} = k_{N\to I} + k_{I\to N} = 1276.7 \pm 173\ s^{-1}$ and presenting a population of 1.89 ± 0.16% for the high energy conformational state.

D145E Behavior in Reconstituted Fibers—To evaluate the mutant and WT forms of cTnC for their affinity for the thin

TABLE 2
ESI-MS analysis of WT and D145E
Act., actual; Iso., isotope; Pred., predicted.

Component	Mass[a]	Molecule	Abundance	Abundance	S.D.	Act. peak	z	Iso. mass	Pred. peak
				%					
Apo-WT	18,756.6	[M+H]+	195,900	100	0.88	1104.2	17+	18,755.1	1104.3
						1173.3	16+	18,757.9	1173.3
						1251.2	15+	18,754.6	1251.3
						1340.9	14+	18,759.9	1340.9
						1443.5	13+	18,753.5	1443.6
						1564.2	12+	18,758.9	1564.1
Holo-WT	18,873.4	[M+H]+	144,355	100	0.79	1573.8	12+	18,874.5	1573
						1716.8	11+	18,873.9	1715.8
						1887.9	10+	18,870.1	1887
Apo-D145E	18,941.6	[M+H]+	143,517	100	0.37	1353.8	14+	18,940.8	1354.6
						1457.8	13+	18,940.1	1458.7
						1579.3	12+	18,941.4	1580.2
						1722.8	11+	18,941	1723.7
						1894.0	10+	18,940.2	1896
Holo-D145E	18,982.7	[M+H]+	159,887	100	0.55	1356.9	14+	18,983.6	1356.9
						1461.1	13+	18,981.8	1461.1
						1582.8	12+	18,982.9	1582.8

[a] Peak averaged mass.

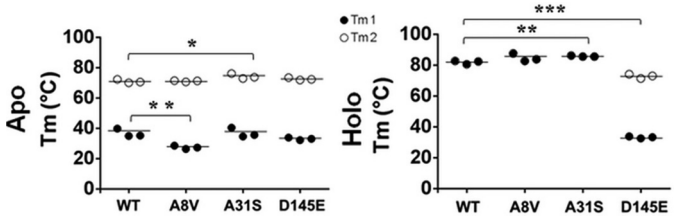

FIGURE 6. **Melting temperatures (T_m) for WT and three mutants in apo- and holo-states obtained by fitting to a two-transition model.** *Points* represent the T_m values of independent experiments ($n = 3$). *, significantly different from WT ($p < 0.05$); **, ($p < 0.01$); and ***, ($p < 0.001$).

filament, experiments were carried out with skinned papillary muscles depleted of their native cTnC and reconstituted with one of the two cTnC isoforms. Dissociation of D145E from the thin filament was much slower compared with the WT, indicating a higher affinity for the thin filament (Fig. 11*A*). The cTnC concentration required for half-maximal binding to the thin filament was about 3-fold greater with the WT protein (0.3 *versus* 0.1 μM), again indicating a higher affinity of D145E for the thin filament (Fig. 11*B*).

Discussion

TNNC1 is now included in routine genetic screening for HCM mutations (15), but up to this point there has appeared very little structural information showing how these mutations affect the binding affinity of cTnC for Ca^{2+} and for its protein partners on the thin filament. Cardiomyopathic mutations can be found in both domains of the protein, but they all share a unifying molecular mechanism: accompanied by minimal changes in overall structure, they affect site II Ca^{2+} binding affinity and kinetics when cTnC is incorporated into the thin filament. It is widely recognized that both domains of cTnC can communicate with each other; however, we still do not know how the information is transmitted from one domain to the other.

CPMG-RD measurements have proven useful for probing the population and exchange rates of marginally stable and/or destabilized mutants (16). The short lifetimes and small populations of these excited conformers present researchers with a difficult task when only conventional structural biology techniques are available. Innovative CPMG-RD applications, either alone or in combination with physical approaches such as high hydrostatic pressure (17), are currently emerging as tools for understanding the molecular mechanisms of protein folding and misfolding (18, 19) and protein functionalities (20). Here, our CPMG-RD measurements captured a low populated, high energy conformer of marginal stability caused by a disease-related mutation in site IV that derails Ca^{2+} coordination at both C-domain sites III and IV. The occurrence of this excited state intermediate does not cause global unfolding but favors a more open C-domain conformation with lower stability and slower internal dynamics in specific segments. As a result, there is an allosteric communication of increased affinity at Ca^{2+}-binding site II of the N-domain, a characteristic feature of the HCM phenotype (21). These features may explain why D145E has a higher affinity for the thin filament and dissociates more slowly from skinned fibers (Fig. 11), as discussed below.

Our first experiments targeted the question of Ca^{2+} binding stoichiometry in the isolated D145E protein, an issue that had been left open in previous reports (4, 13). Here, a clear response to Ca^{2+} was obtained for WT but not D145E in measurements of hydrophobic surface exposure (Fig. 1) and thermal stability (Fig. 6). SAXS experiments in the presence of a subdenaturing urea concentration also revealed a Ca^{2+} response for the WT but not the mutant (Fig. 7*E*). These results are explained by direct measurements of Ca^{2+} binding by ESI-MS showing that both C-domain sites of D145E are inoperative (Figs. 4*C* and 5).

A major distinction between the WT and mutant is evident in the backbone dynamics, captured by conventional relaxation measurements using NMR. Notably, although the fast-exchange (ps-ns) dynamics are for the most part not affected by the mutation (Fig. 9*A*, *lower panel*), a slower exchange process appears and may contribute locally toward the loss of Ca^{2+} binding in site III. Evidence for this contribution comes from D145E C-terminal residues with R_2/R_1 ratios that are systematically higher than those observed for WT, consistent with μs-ms conformational exchange motions (Fig. 9*A*, *upper panel*). In addition, there are repercussions of the mutation for

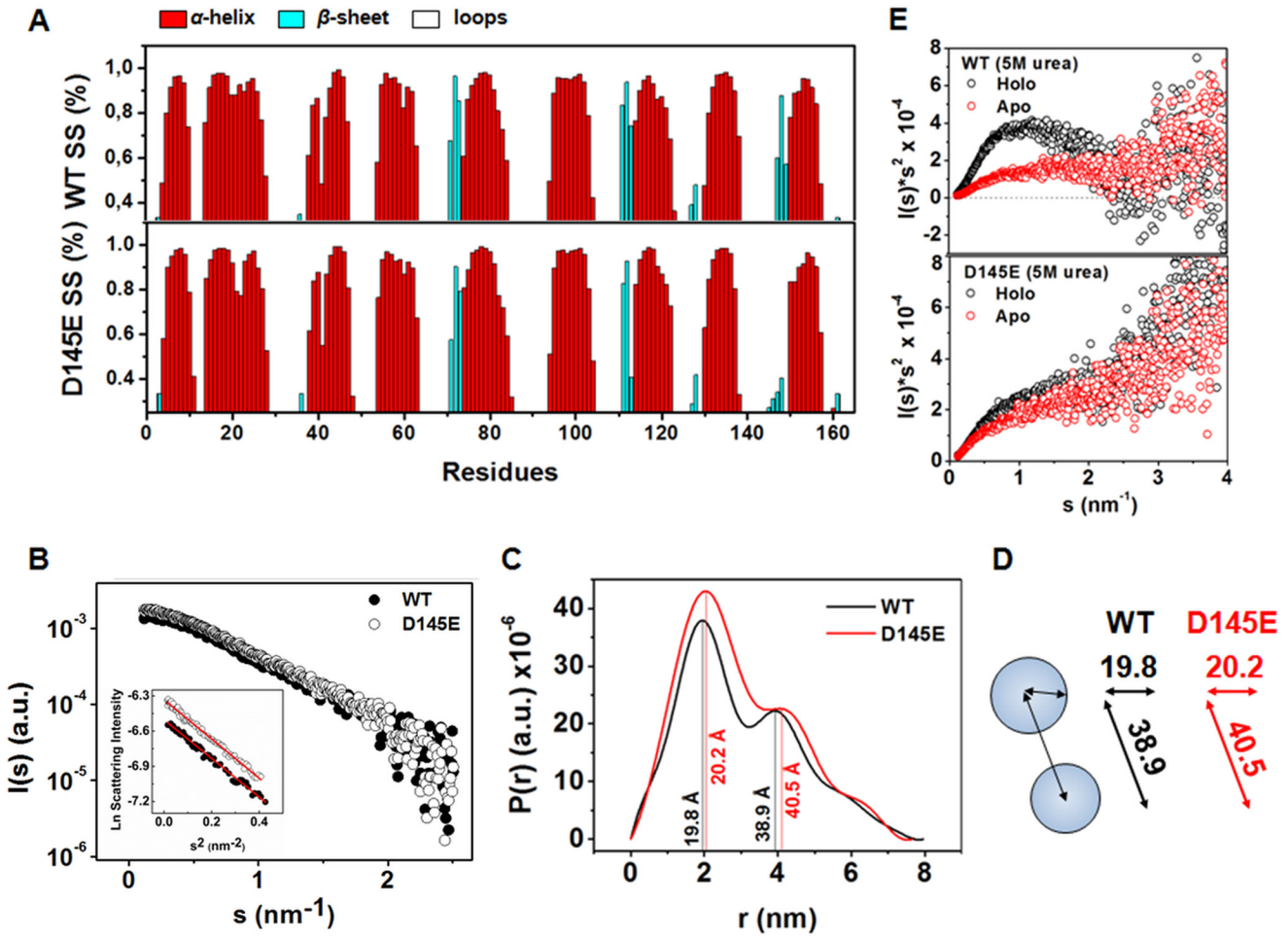

FIGURE 7. **The overall structure of cTnC D145E is similar to WT.** *A*, per-residue secondary structure content (*SS*) obtained from TALOS+ for holo-WT (*upper plot*) and holo-D145E (*lower plot*). α-Helical regions are shown in *red*, β-sheet regions in *cyan*, and loops as *open spaces*. *B*, scattering intensities *I*(*s*) in log scale *versus s* obtained from SAXS for holo-WT (*filled circles*) and holo-D145E (*open circles*). *Inset*, represents Guinier plots for each construct showing no evidence of aggregation. *C*, pair-distance distribution functions of interatomic vectors (*P*(r)) obtained from the scattering intensities for WT (*black*) and D145E (*red*) exhibit the radius of one domain and the distance between two domains (*first* and *second peak*, respectively). *D*, schematic representation of [*P*(*r*)] values for WT and D145E obtained in *C*. *E*, Kratky plots in the presence of 5 M urea for WT (*top*) and D145E (*bottom*) in the presence (*black*) and absence (*red*) of Ca^{2+}.

TABLE 3

Dimensional values obtained by SAXS for cTnC isoforms

Values shown are the best-fit parameters ± S.D. for apo- and holo-states.

	WT		A8V		A31S		D145E	
Constructs	**Apo**	**Holo**	**Apo**	**Holo**	**Apo**	**Holo**	**Apo**	**Holo**
R_g (Å)[a]	28.3 ± 0.2	22.5 ± 0.2	28.7 ± 0.3	22.5 ± 0.2	29 ± 0.2	23.2 ± 0.1	27 ± 0.5	21.9 ± 0.2
R_g (Å)[b]	28.5 ± 0.01	23.6 ± 0.01	27.8 ± 0.01	23.2 ± 0.01	30.2 ± 0.01	23.9 ± 0.01	27.5 ± 0.02	23.3 ± 0.02
D_{max} (Å)[b]	95.1	78.8	87.5	78.7	101.6	79.6	88.4	76.9

[a] R_g, reciprocal space (derived using Guinier approximation).
[b] R_g, real space (calculated using the program GNOM).

the dynamics in αD of the N-domain (Fig. 9*A*) and greater flexibility of the central helix (Fig. 9*D*).

These data are important; they provide evidence for transmission of this altered dynamics from the C- to the N-domain. For skeletal TnC, an inverse correlation exists between protein stability and Ca^{2+} affinity, *i.e.* an increase in protein stability leads to a decrease in Ca^{2+} affinity (22, 23) and vice versa. Intramolecular coupling between the N- and C-domains has been observed for skeletal TnC (24), and several lines of evidence support this cross-talk mechanism (25–28), which is probably aided by the bending of the DE-linker helix (29, 30). Bending at the DE linker is even more pronounced for the cardiac protein (31, 32), and we see the consequences of this N-/C-domain cross-talk in the form of an allosteric event in the N-domain, mitigating in part the potentially catastrophic effects of an HCM-related mutation in the C-domain.

Other studies have analyzed aspects of the internal dynamics of cTnC mutants, restricted to isolated C- or N-domains (33, 34). It is worthwhile comparing the results for D145E with data from the dilated cardiomyopathy mutation G159D located at the end of the C-domain. Unlike D145E, this mutation presents a decrease of Ca^{2+} sensitivity in fibers and myofibrils. Moreover, the G159D mutation triggers different kinetics of conformational transitions (35, 36); it is noteworthy that it also had no

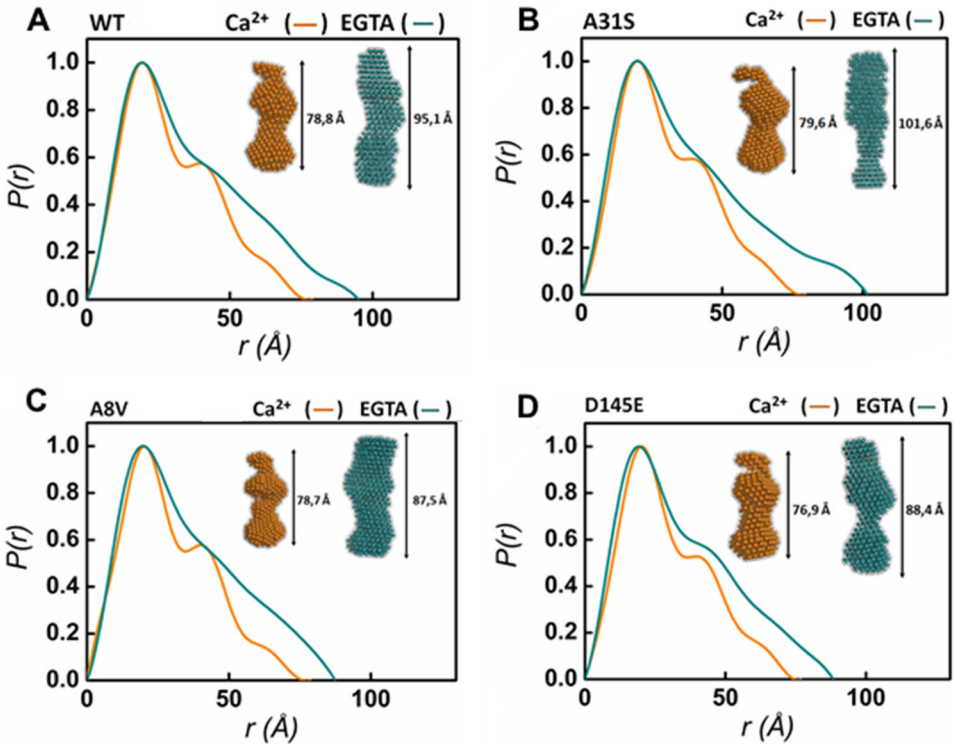

FIGURE 8. **Small-angle X-ray scattering data for WT and cTnC mutants.** *A–D*, relative distance distribution functions (*P*(r)) of mutants in the apo (*dark cyan*)- and holo-states (*orange*) for WT (*A*), A31S (*B*), A8V (*C*), and D145E (*D*), respectively.

effect on local dynamics as measured by experiments like that shown in Fig. 9*A* (33).

The CPMG analysis adds an important dimension to R_2/R_1 relaxation rates. Although R_2/R_1 rates provide initial evidence of an altered local dynamics in the C-domain of D145E, CPMG is sensitive enough to quantify the exchange rates and size of both populations: the major conformer and the low populated excited state present in D145E. Thus D145E appears to be unique in that it inserts a Ca^{2+} binding flaw in the C-domain that has a local impact on protein dynamics through the population of a kinetically trapped excited state. The open conformation, slower motions, and local unfolding of αH in the D145E C-domain, together with the allosteric effect at Ca^{2+}-binding site II of the N-domain, are events that plausibly favor cTnC contacts with other proteins of the thin filament, thereby accounting for this mutant having tighter binding and slower dissociation from skinned fibers (Fig. 12).

Overall, the D145E mutant functions remarkably well in the laboratory; it binds to the thin filament and contributes to full-fledged regulation (both activation and inhibition, including cross-bridges) with only a small increment in Ca^{2+} sensitivity of the N-domain. With regard to the question of global structural changes caused by the D145E mutation, our experiments with skinned fibers provided unexpected evidence for some degree of loose folding of the C-domain. Sites III and IV are traditionally considered "structural" sites, always occupied by Ca^{2+} or Mg^{2+} and essential for maintaining cTnC bound to the thin filament but not involved in beat-to-beat regulation (8). Experiments like that of Fig. 11 provide a means of comparing the efficacy of the C-domain structure in anchoring cTnC to the filament when sites III and IV are altered. Both experiments demonstrated that the D145E mutant has a higher affinity for the thin filament than the WT isoform, even though its C-domain does not bind cations. The D145E C-domain is demonstrably rather open, with an exposed hydrophobic region equivalent to that found for Ca^{2+}-bound WT (Fig. 1*B*). Normally, TnC in skinned fibers requires the presence of Ca^{2+} or Mg^{2+} to induce the formation of a stable complex with its partners on the thin filament. We infer that this mutant has acquired a C-domain conformation that already favors this complex. Thus the C-domain may provide an attractive target for small molecules that have the potential to exert a long distance effect on the Ca^{2+} sensitivity of the N-domain. Furthermore, the proposed allosteric modulation could be extended to TnC orthologs and other EF-hand proteins such as calmodulin or myosin essential light chain. An understanding of how Ca^{2+}-binding proteins change during evolution, preserving (or losing) their ability to regulate biological function, can provide information for the engineering of new molecules. Also, targeting this allosteric mechanism seems uniquely suited to the task of exploring the dynamics and activity of these Ca^{2+} sensors (37–39).

Experimental Procedures

Protein Expression and Purification—The pET-3d vector containing the sequences of human cardiac TnC WT and the constructs (A8V, A31S, and D145E) were inserted into BL21 DE3 *Escherichia coli* strain, plated on semi-solid Luria-Bertani (LB) medium and incubated at 37 °C for ~16 h. The colonies were transferred to 25 ml of LB and placed in a shaker at 37 °C at 180 rpm for 12 h. Next day, 5 ml of the culture was transferred to an Erlenmeyer flask containing 800 ml of LB, and cells were

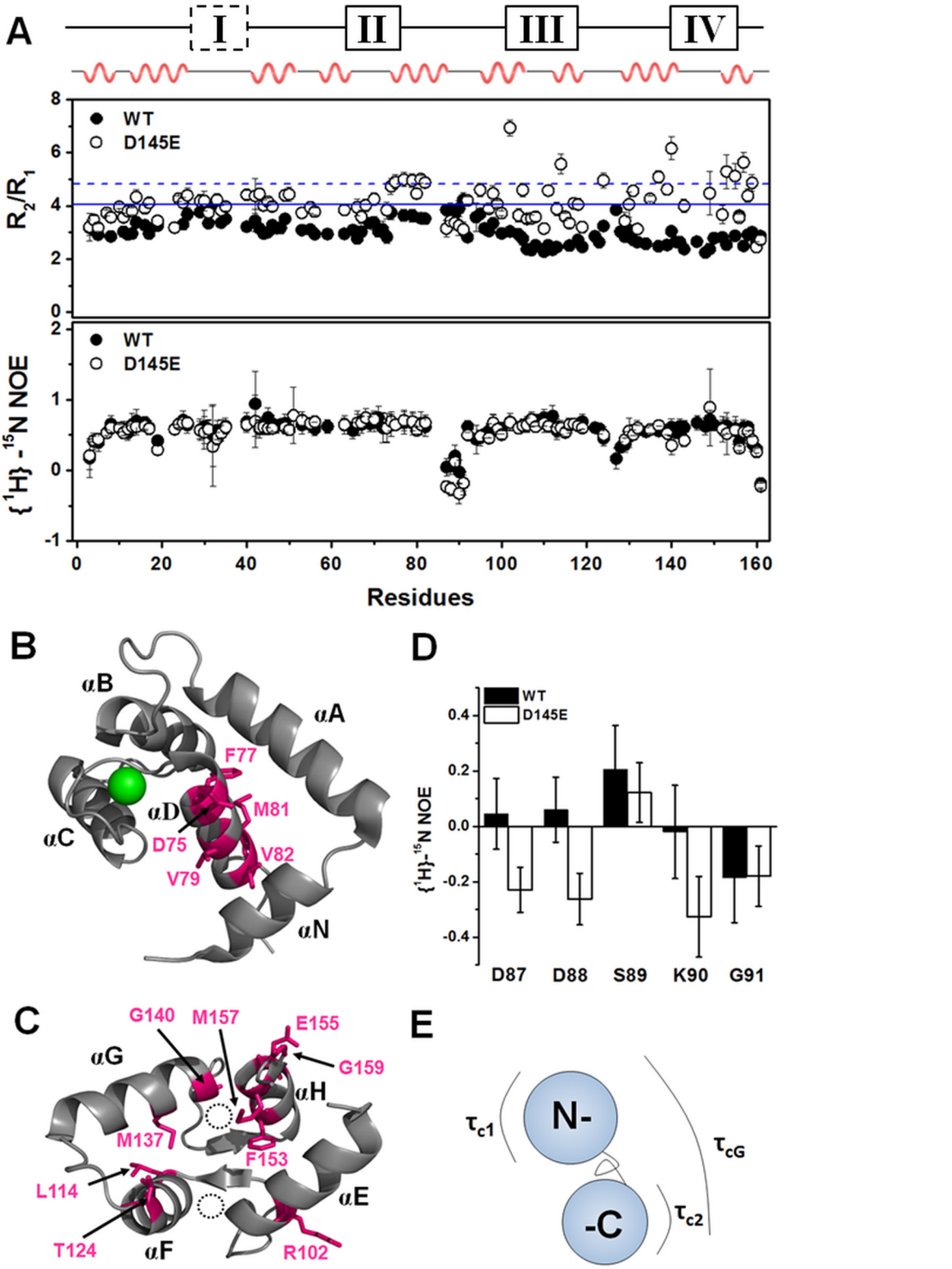

FIGURE 9. **Backbone dynamics of holo-WT and holo-D145E.** *A*, *upper panel*, R_2/R_1 relaxation ratio per residue for WT (*filled circles*) and D145E (*open circles*). The *solid* and *dashed blue lines* represent the R_2/R_1 average values among residues for D145E and 1 S.D. from the average, respectively. Ca^{2+}-binding sites and secondary structure elements are shown schematically along the top; the *dashed box* represents inactive binding site I. *Lower panel*, {^{1}H}-^{15}N NOE data per residue. *B* and *C*, residues of D145E with R_2/R_1 values > average + 1 S.D. are highlighted in *magenta* in the structure of cTnC (PDB code 1J1E). Sites for Ca^{2+} are shown as a *green sphere* in *B* and as *empty circles* in *C*. *D*, {^{1}H}-^{15}N NOE values for the linker residues connecting N- to C-domains. *E*, schematic showing different correlation times (τ_{c1}, τ_{c2}, and τ_{cG}) for the N-domain, the C-domain, and the overall WT cTnC.

grown at 37 °C at 180 rpm until absorbance ($A_{600\,nm}$) reached 0.8–1.0. All cultures contained ampicillin at 50 $\mu g \cdot ml^{-1}$. Induction was achieved with 1 mM isopropyl β-D-1-thiogalactopyranoside followed by additional growth at 37 °C and 180 rpm for 7 h. Samples were centrifuged for 10 min at 8000 × *g* and 4 °C and stored at −20 °C until needed. Lysis was per-

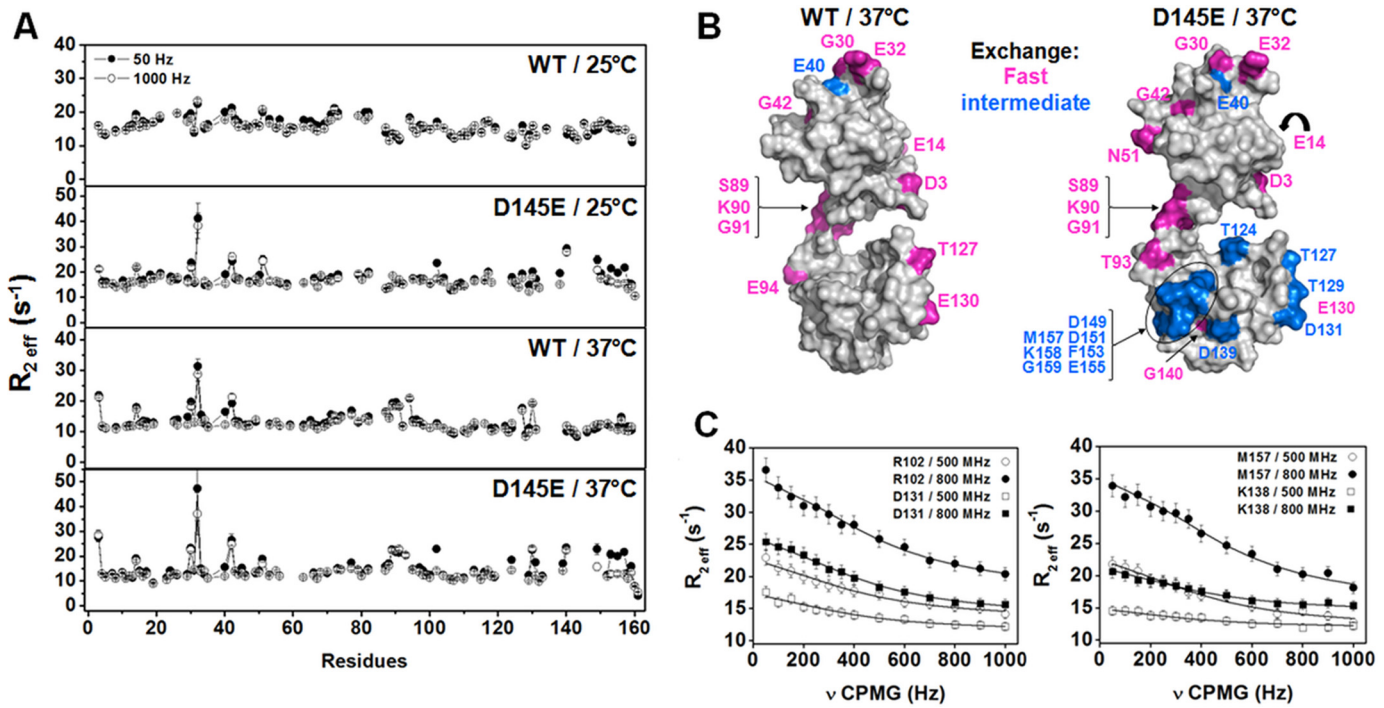

FIGURE 10. **Quantitative analysis of exchange dynamics in D145E.** *A*, R_{2eff} values for each residue obtained by CPMG relaxation dispersion of WT and D145E in the holo-state at 50 Hz (*filled circles*) and 1000 Hz (*open circles*). *Upper panels*, 25 °C; *lower panels*, 37 °C. *B*, residues experiencing intermediate exchange at 37 °C are mapped in *blue* on the surface of the cTnC structure (*gray*) for WT and D145E. Residues mapped in *pink* present fast-exchange rates. *C*, effective transverse relaxation rates ($R_{2,eff}$) at 37 °C plotted as a function of frequency (υ_{CPMG}) for the representative residues Arg-102, Asp-131, Lys-138, and Met-157 at 500 and 800 MHz for holo-D145E (*open* and *filled symbols*, respectively).

formed by sonication in buffer A containing 50 mM Tris-Cl (pH 7.8), 6 M urea, 1 mM EDTA, and 1 mM fresh dithiothreitol (DTT) followed by 20 min at 15,000 × *g* and 4 °C. The supernatant was loaded onto a Q-Sepharose column (coupled to an Äkta Purifier system) equilibrated previously in buffer A. Elution was performed with a linear gradient of 300 ml from 0 to 0.6 M KCl added to buffer A. The most enriched fractions observed at $A_{280\,nm}$ were collected and dialyzed against 50 mM Tris-Cl (pH 7.5), 50 mM NaCl, 1 mM $MgCl_2$, 1 mM $CaCl_2$, and 1 mM DTT and loaded onto a Superdex 75 prep grade column (GE Life Sciences) equilibrated previously in the same buffer. Eluted fractions were concentrated when necessary in a 10,000 MWCO Amicon (EMD Millipore, catalog No. 901024) and stored at −80 °C. ^{15}N- and ^{15}N-^{13}C-labeled proteins were produced as described previously (40) and purified as above.

Fluorescence Spectroscopy—Fluorescence emission was recorded using an ISSK2 spectrofluorometer (ISS Inc., Champaign, IL). For Ca^{2+} titrations, 2 μM of bis-ANS fluorescence was excited at 360 nm and monitored at 490 nm and 15 °C. Microliter amounts of Ca^{2+} (~0.5–2 μl) were added to buffer containing 2 μM protein and 200 mM MOPS (pH 7.0), 150 mM KCl, 2 mM EGTA, and 1 mM DTT (final reaction volume, 3 ml). Titrations between *p*Ca 2.5 and 9.0 at free 2 mM [Mg^{2+}] were calculated using the *p*Ca Calculator suite (41). The pH was 7.0 at the end of titrations. Results were fitted using OriginPro software (Northampton, MA) with the following equation, which describes two classes of binding sites (42),

$$\frac{F}{F_0} = \frac{1 + A_1[Ca^{2+}]^{n1}}{(K_1^{n1} + [Ca^{2+}]^{n1})} + \frac{A_2[Ca^{2+}]}{(K_2 + [Ca^{2+}])} \qquad \text{(Eq. 1)}$$

where F is the fluorescence at each [Ca^{2+}], F_0 is the fluorescence at *p*Ca 9.0, A_1 and A_2 are the magnitudes of transitions, $n1$ is the Hill coefficient, and K_1 and K_2 are [Ca^{2+}] at the midpoints of the two transitions. Experiments are shown as average ± S.E. of three independent experiments using at least two different protein batches.

NMR Spectroscopy—WT and D145E peak assignments were carried out at the Brazilian Biosciences National Laboratory (LNBio), Campinas, Brazil. We acquired a set of three-dimensional experiments ($HNC_\alpha C_\beta$, $C_\beta C_\alpha$(CO)NH, HN(C_α)CO, and HNCO) using ^{15}N-^{13}C-labeled proteins (~0.5–1 mM) at 25 °C in a Varian Inova, 600 MHz, equipped with a triple resonance cryogenic probe. Buffer conditions were 20 mM MOPS (pH 7.0), 6 mM $CaCl_2$, 1 mM $MgCl_2$, 100 mM KCl, and 10 mM DTT containing 10% D_2O. ^{1}H-^{15}N peak assignments are depicted in Figs. 2 and 3. The CARA 1.8.4 platform (Computer Aided Resonance Assignment) was used for assignment. To compare the secondary structure predictions for WT and D145E using the TALOS+ suite (14), we acquired $H_\beta H_\alpha$(CO)NH spectra for both proteins, thus completing the H_α and H_β resonance assignments.

For NMR Ca^{2+} titrations, heteronuclear ^{1}H-^{15}N HSQC NMR spectra were acquired at 25 °C in a Bruker Avance III 800-MHz or 500-MHz spectrometer equipped with a 5-mm TXI probe at the National Center of Nuclear Magnetic Resonance Jiri Jonas (Rio de Janeiro, Brazil). WT and D145E were recorded at *p*Ca 9.7 (apoform), 7, 6.5, 6, 5.8, 5.6, 5.2, 4.5, 3.9, 3.6, 3.3, 3, 2.7, 2.5, and 2. The ^{1}H-^{15}N HSQC spectra were acquired with 1024 increment points for the ^{1}H dimension and 128 points for the ^{15}N dimension, with 16 scans collected at each

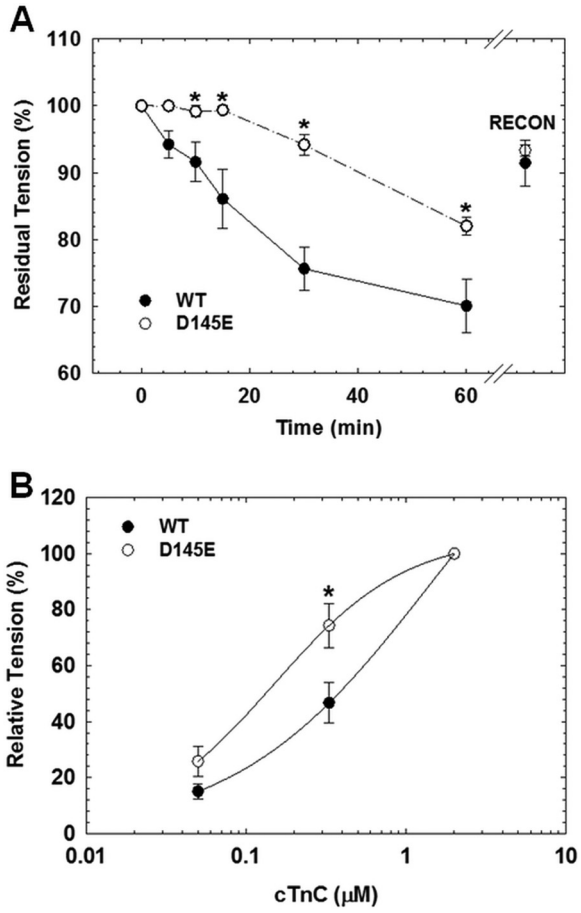

FIGURE 11. **Dissociation from and binding of cTnC D145E to thin filaments in skinned rat cardiac fibers.** *A*, the D145E mutation significantly slows the dissociation of cTnC from the thin filament. Native cTnC was extracted and fibers were reconstituted with human recombinant cTnC WT or D145E. The dissociation of cTnC is represented by the fall in tension after cTnC extraction and reconstitution. *RECON*, tension recovery following incubation with the same protein after the dissociation curve. *B*, the D145E mutation significantly increases cTnC binding affinity to the thin filament. Native cTnC was extracted, and fibers were successively incubated with increasing concentrations of human recombinant cTnC WT or D145E (see "Experimental Procedures" for further details). *, $p < 0.05$ for D145E *versus* WT at the same time point (*A*) or at same cTnC concentration (*B*).

increment. CSP analysis was performed at *p*Ca 2.5 and 6.0 against *p*Ca 7.0 for WT and D145E using the following equation,

$$\mathrm{CSP} = [(\Delta\delta_H)^2 + 0.1(\Delta\delta_N)^2]^{1/2} \quad \text{(Eq. 2)}$$

where $\Delta\delta_H$ and $\Delta\delta_N$ are the chemical shift variations between *p*Ca 2.5 and 7.0 or *p*Ca 6.0 and 7.0 of ^{1}H and ^{15}N, respectively. Protein concentrations for titrations were 0.1–0.3 mM in 200 mM MOPS (pH 7.0), 150 mM KCl, 2 mM EGTA, 2 mM free Mg^{2+}, and 1 mM DTT. All spectra were processed using Topspin 3.2, and chemical shift values were measured using the software CCPN Analysis 2.4.1.

Mass Spectrometry—Samples were analyzed with a high capacity ion trap LC/MSn system HCT Ultra ETD (Bruker Daltonik, Germany) equipped with a standard ESI ion source with full scan data in UltraScan mode between *m*/*z* 400 and 3000, in positive mode and with a fixed accumulation time of 30 ms. The ionization parameters of nebulizer gas, dry gas, and dry temperature were 230 psi, 5 liters · min^{-1}, and 300 °C, respectively. The ion spray voltage was set to 2500 V, and the maximal accumulation time was set to 200 ms. Extracted ion chromatograms were used for identification of the expected molecular weights. All data were acquired and processed using Compass 1.3 software (Bruker Daltonik, Bremen, Germany). Calculations including calibration curve regressions, sample concentrations, and statistics were performed using GraphPad Prism 5.0 software (GraphPad, San Diego, CA). Protein concentration was 100 μM in 200 mM MOPS (pH 7.0), 150 mM KCl, and 2 mM EGTA (for the apocondition) and 4 mM $CaCl_2$ (for the holocondition).

Circular Dichroism Spectropolarimetry—To measure the effects of cTnC mutations on protein stability, thermograms ranging from 20 to 90 °C were performed in a Chirascan spectropolarimeter (Applied Photophysics). Samples were heated at a rate of 1 °C · min^{-1} in a quartz cell of 1-mm path length, and ellipticity was recorded at 222 nm every 0.2 °C. Mean residue ellipticities $(\theta)_{MRE}$ in deg · cm^2 · $dmol^{-1}$ · res^{-1} were calculated using the following equation,

$$(\theta)_{MRE} = \theta \frac{\left[0.1\left(\frac{MW}{n}\right)\right]}{lc} \quad \text{(Eq. 3)}$$

where θ is the measured ellipticity in millidegrees, MW is the molecular weight in Daltons, n is the number of residues in the primary sequence, l is the path length in cm, and c the concentration in mg · ml^{-1}. Reversibility was observed for all transitions, and experimental points were fitted using the following biphasic dose-response function in OriginPro,

$$y = A_1 + (A_2 - A_1)\left[\frac{p}{1 + 10^{(\log x01 - x)h1}} + \frac{1-p}{1 + 10^{(\log x02 - x)h2}}\right] \quad \text{(Eq. 4)}$$

where A_1 and A_2 are the bottom and top plateau values, log×01 and log×02 are the temperatures at the first and second midpoint transitions, h_1 and h_2 are Hill slopes, and p is a proportion factor. The protein concentration was 0.1 mg · ml^{-1}, and the buffer contained 20 mM MOPS (pH 7.0), 100 mM KCl, and 1 mM EGTA (for the apocondition) and in addition 2.075 mM $MgCl_2$ and 1.096 mM $CaCl_2$ to yield a free [Ca^{2+}] of 10^{-4} M and a free [Mg^{2+}] of 2 mM (for the holocondition). Results are shown as the average ± S.E. of three independent experiments from at least two different protein batches.

X-ray Scattering Data Collection and Analysis—SAXS measurements were collected on the SAXS1 beamline of the National Synchrotron Light Laboratory (Campinas, Brazil) using a parallel mica sample holder, a Pilatus 300K detector (Dectris, Switzerland), and a wavelength of 0.155 nm at 20 °C. Isolated cTnC mutants were scattered at an *s* range of 0.11 to 4.07 nm^{-1}. Scattering was performed by taking six frames of 5 s with a time delay of 2 s. In buffer alone, a single frame of 100 s was taken. Individual frames from scattered proteins were superimposed and visually inspected prior to averaging. Because no radiation effects were observed among successive frames, averaged values were used to enhance the signal-to-

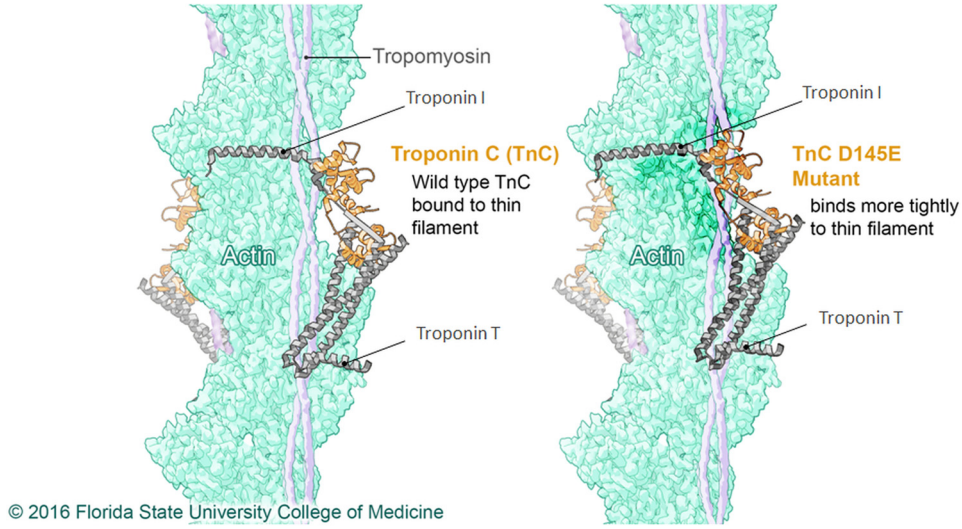

FIGURE 12. **Illustration of the structural effects of D145E on thin filaments.** The proposed allosteric mechanism of Ca^{2+} binding with higher affinity to the N-domain site II due to a loose D145E C-terminal domain is presumably transferred through the connecting elements, linker D/E and αD, and is extended to a higher affinity of D145E to the thin filament (*dark green*). The structure of actin-tropomyosin was obtained from PDB 4A7F. The structure of the core domain of troponin complex was obtained from PDB 1J1E.

noise ratio. Parasitic scattering from the mica sample holder and buffer was properly subtracted from the corresponding protein scattering curve. Buffer contained 200 mM MOPS (pH 7.0), 100 mM KCl, and 1 mM EGTA (for the apocondition) and in addition 2.075 mM $MgCl_2$ and 1.096 mM $CaCl_2$ to yield a free [Ca^{2+}] of 10^{-4} M and free [Mg^{2+}] of 2 mM (for the holocondition) without or with 5 M urea. Protein concentrations ranged from 2 to 4 mg · ml^{-1}.

Subtracted intensities were fitted using autoGNOM (PrimusQt suite) in which an indirect Fourier transformation routine is implemented to obtain the pair distance distribution function, $P(r)$. The radii of gyration (R_g) were computed from Guinier plots using the angular coefficient (α) of the low s region ($s < 1.3/R_g$) and checked against those derived from the $P(r)$ function.

Ab Initio Shape Restorations from Scattering Data—The GASBOR software (43) provided by the ATSAS package is suitable for *ab initio* reconstructions using dummy residues and was chosen for modeling cTnC variants. For each model, 10 runs were generated in GASBOR considering 161 dummy residues in the asymmetric part, no symmetry ($P1$), and scattering intensity as the mode selected for fitting. Models were superimposed by SUPCOMB and averaged using DAMAVER. The normalized spatial discrepancy (NSD) was used as a filter to include models in the averaging procedure. The inclusion criterion derived from NSD was NSD < mean NSD + 2* variation.

Protein Dynamics—The diffusion properties of cTnC WT and D145E were obtained at 37 °C from the longitudinal (R_1) and transverse (R_2) relaxation rates. R_1 and R_2 values were measured from ^1H-^{15}N heteronuclear correlation spectra acquired with relaxation delays of 20, 50, 100, 200, 250, 500, 750, 1000, and 1500 ms and 16, 48, 80, 112, 144, 176, 208, 240, 272, and 304 ms, respectively. {^1H}-^{15}N NOE were obtained from the ratio of peak intensities with and without saturation of the amide protons.

CPMG relaxation dispersion experiments were acquired on Bruker 500- and 800-MHz spectrometers at 25 and 37 °C. Relaxation rates (R_{2eff} (s^{-1})) were calculated from the intensities of resonances in ^1H-^{15}N correlation spectra acquired with different CPMG frequencies (υ_{CPMG}: 50, 100, 150, 200, 250, 300, 350, 400, 500, 600, 700, 800, 900, and 1000 Hz) using the following equation,

$$R_{2eff} = -\frac{1}{T}\ln\left(\frac{I_0}{I_{CPMG}}\right) \quad \text{(Eq. 5)}$$

where T is the relaxation time, I_0 and I_{CPMG} are the intensities of resonances obtained from experiments without and with the CPMG pulse block, and R_{2eff} were plotted as a function of υ_{CPMG} values. The experimental set of data displaying pronounced relaxation dispersion profiles consisted of 11 residues (Arg-102, Thr-127, Thr-129, Asp-131, Asp-132, Lys-138, Asp-149, Tyr-150, Phe-153, Met-157, and Lys-158) and were fit to a model of two-site exchange (44) between the intermediate excited state (I) and the native state (N), $N \leftrightarrow I$, to extract the population of the intermediate state (p_b) and the interconversion rate ($k_{N\rightarrow I}$). The exchange rate constant, K_{ex} (*i.e.* $K_{ex} = k_{N\rightarrow I} + k_{I\rightarrow N}$), was obtained by the following equation.

$$K_{ex} = k_{N\rightarrow I}/P_b \quad \text{(Eq. 6)}$$

Optimization of the theoretical model was carried out using the software CPMG_FIT9 (19) and minimizing the equation,

$$\chi^2 = \sum_{j=1}^{N}\sum_{k=1}^{N}\frac{[R_{2eff}^{calc}(K_{ex}, P_a, P_b, \Delta\omega, R_2) - R_{2eff}^{exp}]^2}{(\Delta R_{2eff}^{exp})^2} \quad \text{(Eq. 7)}$$

where superscripts *calc* and *exp* refer to the theoretical and experimental relaxation rates, respectively. All experiments were carried out in 200 mM MOPS (pH 7.0), 150 mM KCl, 2 mM EGTA, 2 mM free Mg^{2+}, and 1 mM DTT at *p*Ca 2.5.

Experiments with Fibers—The rates of association and dissociation of cTnC to and from the thin filaments were evaluated in permeabilized papillary muscles dissected from the left ventricle of Wistar rats, prepared as described (45) with a protease inhibitor mixture (1% w/v) and Triton X-100 (1% w/v) dissolved in relaxing solution (20 mM imidazole (pH 7.0), 152 mM potas-

sium propionate, 2.5 mM magnesium acetate, 5 mM EGTA, and 2.5 mM K_2Na_2ATP) made up in 50% glycerol. After 24 h at −20 °C, fibers were transferred to a solution without Triton X-100 and stored at −20 °C for up to 2 weeks. Prior to performing assays for binding or dissociation of cTnC, a bundle (~200-μm diameter) was attached to the transducer and stretched to 1.2× rest length for an initial force measurement at *p*Ca 4.4 (*P*(*o*)). All subsequent measurements were made with temperature control (15 °C) and rapid stirring. Native cTnC was extracted using 15-s exposures to Rigor solution containing 0.5 mM trifluoperazine, 20 mM imidazole (pH 6.9), 165 mM potassium propionate, and 10 mM EDTA alternating with 15 s in relaxing solution (see above but without glycerol) for 40 min. After extensive washing to remove trifluoperazine, extraction of native TnC was verified by recording the residual tension at *p*Ca 4.4 (20 mM imidazole (pH 7.0), 152 mM potassium propionate, 6 mM magnesium acetate, 5 mM Ca-EGTA, and 4.4 mM K_2Na_2ATP). For the binding experiments, the residual force values post-extraction were 10.5 ± 2.0 and 6.3 ± 1.9% (*P*/*P*(*o*)) for fibers reconstituted with WT and D145E, respectively. For the dissociation experiments, the residual force values post-extractions were 11.9 ± 4.7 and 21.0 ± 5.7% (*P*/*P*(*o*)) for fibers reconstituted with WT and D145E, respectively.

For estimates of HcTnC affinity for the thin filament, binding curves were constructed using 0.025–2 μM WT or D145E cTnC to reconstitute papillary fibers in relaxing solution adjusted to 2 mM free Mg^{2+} without Ca^{2+} (20 mM imidazole (pH 7.0), 152 mM potassium propionate, 6.4 mM magnesium acetate, 5 mM EGTA, 4.4 mM K_2Na_2ATP, and 1 mM DTT). Successive 20-min incubations at a low concentration of cTnC were followed by tests at *p*Ca 4.4 until no further increment in tension occurred. The procedure was repeated with a second, higher concentration of protein and, finally, with a drop of protein (55 μM) applied directly to the fiber for 1 min (in air). These values were no greater than those obtained by incubation with 2 μM protein, indicating saturation of the TnC-binding sites at 2 μM. On average, force recovery after this step was 67.4 ± 2.8% (WT) and 70.1 ± 2.9% (D145E) of the original *P*(*o*) value with native cTnC and was not different for the two recombinant proteins.

For dissociation of cTnC from the thin filament, fibers were depleted of native cTnC and reconstituted immediately with a drop of protein (55 μM) applied directly to the fiber. The reconstitution values prior to the dissociation curves were 72.1 ± 4.7 and 86.7 ± 4.4% (*P*/*P*(*o*)) for WT and D145E, respectively. When a test with *p*Ca 4.4 revealed saturation of the cTnC-binding sites, the fiber was exposed to a relaxing solution buffered with EDTA to contain 0.1 mM MgATP and 1 μM free Mg^{2+} (20 mM imidazole (pH 7.0), 43 mM potassium propionate, 2.3 mM magnesium acetate, 10 mM EDTA, and 1.6 mM K_2Na_2ATP). This Mg^{2+} concentration is well below that required to occupy the C-domain sites. This solution was used because cTnC binds to the cardiac thin filament with a very high affinity, and in the absence of divalent cations bound to C-domain sites, cTnC dissociation can be measured in shorter time spans preventing any effect of fiber rundown. Dissociation of WT and D145E cTnC in this solution was tested using brief applications of *p*Ca 4.4 to record the loss of isometric tension over a period of 60 min followed by a final reconstitution with a drop of the recombinant protein to ascertain recovery. On average, this value was 91.5 ± 3.4% (WT) and 86.7 ± 4.4% (D145E) of the original force recorded initially with cTnC in the fiber, and it was not different for the two recombinant proteins.

Statistical Analysis—The results for statistical analysis are shown as the average ± S.E. of at least three independent experiments. Statistical significance of affinity constants (K_1 and K_2) extracted from the fit of bis-ANS and skinned fiber binding and dissociation assays were tested using unpaired Student's test against the WT protein. Melting temperatures (T_m) obtained from the fit of circular dichroism thermograms were tested for statistical significance using one-way analysis of variance followed by Dunnett's test for post-hoc comparisons. *p* values lower than 0.05 were considered significantly different and are described throughout this article.

Author Contributions—M. d. A. M., J. R. P., and G. A. P. d. O. designed the research, and M. d. A. M., G. A. P. d. O., A. H. M., M. T. Q. d. M. and J. M. performed the research. J. L. S., M. M. P., and A. I. contributed new reagents/analytic tools. M. d. A. M., G. A. P. d. O., J. M., J. R. P., A. H. M., M. T. Q. d. M., and M. M. S. analyzed the data; and M. d. A. M., G. A. P. d. O., J. R. P., J. L. S. and M. M. S. wrote the paper.

References

1. Lan, F., Lee, A. S., Liang, P., Sanchez-Freire, V., Nguyen, P. K., Wang, L., Han, L., Yen, M., Wang, Y., Sun, N., Abilez, O. J, Hu, S., Ebert, A. D., Navarrete, E. G., Simmons, C. S., *et al.* (2013) Abnormal calcium handling properties underlie familial hypertrophic cardiomyopathy pathology in patient-specific induced pluripotent stem cells. *Cell Stem Cell* **12,** 101–113
2. Writing Group Members, Mozaffarian, D., Benjamin, E. J., Go, A. S., Arnett, D. K., Blaha, M. J., Cushman, M., Das, S. R., de Ferranti, S., Després, J. P., Fullerton, H. J., Howard, V. J., Huffman, M. D., Isasi, C. R., Jiménez, M. C., Judd, S. E., *et al.* (2016) Heart disease and stroke statistics-2016 update: a report from the American Heart Association. *Circulation* **133,** e38–e60
3. Maron, B. J., Towbin, J. A., Thiene, G., Antzelevitch, C., Corrado, D., Arnett, D., Moss, A. J., Seidman, C. E., Young, J. B., American Heart Association, Council on Clinical Cardiology, Heart Failure and Transplantation Committee, Quality of Care and Outcomes Research and Functional Genomics and Translational Biology Interdisciplinary Working Groups, and Council on Epidemiology and Prevention (2006) Contemporary definitions and classification of the cardiomyopathies: an American Heart Association Scientific Statement from the Council on Clinical Cardiology, Heart Failure and Transplantation Committee; Quality of Care and Outcomes Research and Functional Genomics and Translational Biology Interdisciplinary Working Groups; and Council on Epidemiology and Prevention. *Circulation* **113,** 1807–1816
4. Landstrom, A. P., Parvatiyar, M. S., Pinto, J. R., Marquardt, M. L., Bos, J. M., Tester, D. J., Ommen, S. R., Potter, J. D., and Ackerman, M. J. (2008) Molecular and functional characterization of novel hypertrophic cardiomyopathy susceptibility mutations in TNNC1-encoded troponin C. *J. Mol. Cell. Cardiol.* **45,** 281–288
5. Parvatiyar, M. S., Landstrom, A. P., Figueiredo-Freitas, C., Potter, J. D., Ackerman, M. J., and Pinto, J. R. (2012) A mutation in TNNC1-encoded cardiac troponin C, TNNC1-A31S, predisposes to hypertrophic cardiomyopathy and ventricular fibrillation. *J. Biol. Chem.* **287,** 31845–31855
6. Potter, J. D., and Gergely, J. (1975) The calcium and magnesium binding sites on troponin and their role in the regulation of myofibrillar adenosine triphosphatase. *J. Biol. Chem.* **250,** 4628–4633

7. Li, M. X., Spyracopoulos, L., and Sykes, B. D. (1999) Binding of cardiac troponin-I147–163 induces a structural opening in human cardiac troponin-C. *Biochemistry* **38,** 8289–8298
8. Holroyde, M. J., Robertson, S. P., Johnson, J. D., Solaro, R. J., and Potter, J. D. (1980) The calcium and magnesium binding sites on cardiac troponin and their role in the regulation of myofibrillar adenosine triphosphatase. *J. Biol. Chem.* **255,** 11688–11693
9. Herzberg, O., and James, M. N. (1985) Structure of the calcium regulatory muscle protein troponin-C at 2.8 A resolution. *Nature* **313,** 653–659
10. Marques, M. A., and de Oliveira, G. A. (2016) Cardiac troponin and tropomyosin: structural and cellular perspectives to unveil the hypertrophic cardiomyopathy phenotype. *Front. Physiol.* **7,** 429
11. Pinto, J. R., Parvatiyar, M. S., Jones, M. A., Liang, J., Ackerman, M. J., and Potter, J. D. (2009) A functional and structural study of troponin C mutations related to hypertrophic cardiomyopathy. *J. Biol. Chem.* **284,** 19090–19100
12. Cordina, N. M., Liew, C. K., Gell, D. A., Fajer, P. G., Mackay, J. P., and Brown, L. J. (2013) Effects of calcium binding and the hypertrophic cardiomyopathy A8V mutation on the dynamic equilibrium between closed and open conformations of the regulatory N-domain of isolated cardiac troponin C. *Biochemistry* **52,** 1950–1962
13. Swindle, N., and Tikunova, S. B. (2010) Hypertrophic cardiomyopathy-linked mutation D145E drastically alters calcium binding by the C-domain of cardiac troponin C. *Biochemistry* **49,** 4813–4820
14. Shen, Y., Delaglio, F., Cornilescu, G., and Bax, A. (2009) TALOS+: a hybrid method for predicting protein backbone torsion angles from NMR chemical shifts. *J. Biomol. NMR* **44,** 213–223
15. Maron, B. J., Maron, M. S., and Semsarian, C. (2012) Genetics of hypertrophic cardiomyopathy after 20 years: clinical perspectives. *J. Am. Coll. Cardiol.* **60,** 705–715
16. Korzhnev, D. M., and Kay, L. E. (2008) Probing invisible, low-populated states of protein molecules by relaxation dispersion NMR spectroscopy: an application to protein folding. *Acc. Chem. Res.* **41,** 442–451
17. Tugarinov, V., Libich, D. S., Meyer, V., Roche, J., and Clore, G. M. (2015) The energetics of a three-state protein folding system probed by high-pressure relaxation dispersion NMR spectroscopy. *Angew. Chem. Int. Ed. Engl.* **54,** 11157–11161
18. Korzhnev, D. M., Kloiber, K., and Kay, L. E. (2004) Multiple-quantum relaxation dispersion NMR spectroscopy probing millisecond time-scale dynamics in proteins: theory and application. *J. Am. Chem. Soc.* **126,** 7320–7329
19. Korzhnev, D. M., Religa, T. L., Banachewicz, W., Fersht, A. R., and Kay, L. E. (2010) A transient and low-populated protein-folding intermediate at atomic resolution. *Science* **329,** 1312–1316
20. De Simone, A., Aprile, F. A., Dhulesia, A., Dobson, C. M., and Vendruscolo, M. (2015) Structure of a low-population intermediate state in the release of an enzyme product. *Elife* **4,** e02777
21. Willott, R. H., Gomes, A. V., Chang, A. N., Parvatiyar, M. S., Pinto, J. R., and Potter, J. D. (2010) Mutations in troponin that cause HCM, DCM and RCM: what can we learn about thin filament function? *J. Mol. Cell. Cardiol.* **48,** 882–892
22. Grabarek, Z., Mabuchi, Y., and Gergely, J. (1995) Properties of troponin C acetylated at lysine residues. *Biochemistry* **34,** 11872–11881
23. Suarez, M. C., Machado, C. J., Lima, L. M., Smillie, L. B., Pearlstone, J. R., Silva, J. L., Sorenson, M. M., and Foguel, D. (2003) Role of hydration in the closed-to-open transition involved in Ca2+ binding by troponin C. *Biochemistry* **42,** 5522–5530
24. de Oliveira, G. A., Rocha, C. B., Marques, M. de A., Cordeiro, Y., Sorenson, M. M., Foguel, D., Silva, J. L., and Suarez, M. C. (2013) Insights into the intramolecular coupling between the N- and C-domains of troponin C derived from high-pressure, fluorescence, nuclear magnetic resonance, and small-angle X-ray scattering studies. *Biochemistry* **52,** 28–40
25. Grabarek, Z., Leavis, P. C., and Gergely, J. (1986) Calcium binding to the low affinity sites in troponin C induces conformational changes in the high affinity domain: a possible route of information transfer in activation of muscle contraction. *J. Biol. Chem.* **261,** 608–613
26. She, M., Dong, W. J., Umeda, P. K., and Cheung, H. C. (1998) Tryptophan mutants of troponin C from skeletal muscle: an optical probe of the regulatory domain. *Eur. J. Biochem.* **252,** 600–607
27. Moncrieffe, M. C., Venyaminov, S. Y., Miller, T. E., Guzman, G., Potter, J. D., and Prendergast, F. G. (1999) Optical spectroscopic characterization of single tryptophan mutants of chicken skeletal troponin C: evidence for interdomain interaction. *Biochemistry* **38,** 11973–11983
28. Wang, X., Li, M. X., Spyracopoulos, L., Beier, N., Chandra, M., Solaro, R. J., and Sykes, B. D. (2001) Structure of the C-domain of human cardiac troponin C in complex with the Ca2+ sensitizing drug EMD 57033. *J. Biol. Chem.* **276,** 25456–25466
29. Vassylyev, D. G., Takeda, S., Wakatsuki, S., Maeda, K., and Maéda, Y. (1998) Crystal structure of troponin C in complex with troponin I fragment at 2.3-A resolution. *Proc. Natl. Acad. Sci. U.S.A.* **95,** 4847–4852
30. Vinogradova, M. V., Stone, D. B., Malanina, G. G., Karatzaferi, C., Cooke, R., Mendelson, R. A., and Fletterick, R. J. (2005) Ca(2+)-regulated structural changes in troponin. *Proc. Natl. Acad. Sci. U.S.A.* **102,** 5038–5043
31. Cordina, N. M., Liew, C. K., Gell, D. A., Fajer, P. G., Mackay, J. P., and Brown, L. J. (2012) Interdomain orientation of cardiac Troponin C characterized by paramagnetic relaxation enhancement NMR reveals a compact state. *Protein Sci.* **21,** 1376–1387
32. Takeda, S., Yamashita, A., Maeda, K., and Maéda, Y. (2003) Structure of the core domain of human cardiac troponin in the Ca(2+)-saturated form. *Nature* **424,** 35–41
33. Baryshnikova, O. K., Robertson, I. M., Mercier, P., and Sykes, B. D. (2008) The dilated cardiomyopathy G159D mutation in cardiac troponin C weakens the anchoring interaction with troponin I. *Biochemistry* **47,** 10950–10960
34. Robertson, I. M., Sevrieva, I., Li, M. X., Irving, M., Sun, Y. B., and Sykes, B. D. (2015) The structural and functional effects of the familial hypertrophic cardiomyopathy-linked cardiac troponin C mutation, L29Q. *J. Mol. Cell. Cardiol.* **87,** 257–269
35. Dweck, D., Hus, N., and Potter, J. D. (2008) Challenging current paradigms related to cardiomyopathies: are changes in the Ca2+ sensitivity of myofilaments containing cardiac troponin C mutations (G159D and L29Q) good predictors of the phenotypic outcomes? *J. Biol. Chem.* **283,** 33119–33128
36. Dong, W. J., Xing, J., Ouyang, Y., An, J., and Cheung, H. C. (2008) Structural kinetics of cardiac troponin C mutants linked to familial hypertrophic and dilated cardiomyopathy in troponin complexes. *J. Biol. Chem.* **283,** 3424–3432
37. Williams, M. R., Lehman, S. J., Tardiff, J. C., and Schwartz, S. D. (2016) Atomic resolution probe for allostery in the regulatory thin filament. *Proc. Natl. Acad. Sci. U.S.A.* **113,** 3257–3262
38. Fromherz, S., and Szent-Györgyi, A. G. (1995) Role of essential light chain EF hand domains in calcium binding and regulation of scallop myosin. *Proc. Natl. Acad. Sci. U.S.A.* **92,** 7652–7656
39. Dokholyan, N. V. (2016) Controlling allosteric networks in proteins. *Chem Rev.* **116,** 6463–6487
40. Tugarinov, V., Kanelis, V., and Kay, L. E. (2006) Isotope labeling strategies for the study of high-molecular-weight proteins by solution NMR spectroscopy. *Nat. Protoc.* **1,** 749–754
41. Dweck, D., Reyes-Alfonso, A. Jr., and Potter, J. D. (2005) Expanding the range of free calcium regulation in biological solutions. *Anal. Biochem.* **347,** 303–315
42. Pan, B. S., and Johnson, R.G. Jr. (1996) Interaction of cardiotonic thiadiazinone derivatives with cardiac troponin C. *J. Biol. Chem.* **271,** 817–823
43. Svergun, D. I., Petoukhov, M. V., and Koch, M. H. (2001) Determination of domain structure of proteins from X-ray solution scattering. *Biophys. J.* **80,** 2946–2953
44. Carver, J. P., and Richards, R. E. (1972) A general two-site solution for the chemical exchange produced dependence of T2 upon the Carr-Purcell pulse separation. *J. Magn. Reson.* **6,** 89–105
45. Hannon, J. D., Martyn, D. A., and Gordon, A. M. (1992) Effects of cycling and rigor crossbridges on the conformation of cardiac troponin C. *Circ. Res.* **71,** 984–991